文章编号：1001-9014(2026)01-0097-06

DOI:10. 11972/j. issn. 1001-9014. 2026. 01. 011

Effect of extrinsic resistance on noise performance for deep submicron MOSFET

GAO Han-Qi, JIN Jing, ZHOU Jian-Jun*

(School of Electronic Information and Electrical Engineering, Shanghai Jiao Tong University, Shanghai 200240, China)

Abstract: This paper investigates the impact of extrinsic resistance on the noise performance of deep submicron MOSFETs (metal-oxide-semiconductor field-effect-transistor) using the noise correlation matrix method. Analytical closed-form expressions for calculating the four noise parameters are derived based on the small-signal and noise-equivalent circuit models. The results show strong agreement between simulated and experimental data for MOSFETs with a gate length of 40 nm and dimensions of 4×5 μm (number of gate fingers × unit gate width.

Key words: equivalent circuits, MOSFET, parameter extraction, noise model, small signal model

外延电阻对深亚微米MOSFET噪声性能的影响

高涵祺, 金 晶, 周健军*

(上海交通大学 集成电路学院/信息与电子工程学院 模拟射频集成电路设计中心,上海 200240)

摘要:本文采用噪声相关矩阵法,研究了外电路电阻对深亚微米 MOSFET 噪声性能的影响。基于小信号等效电路模型和噪声等效电路模型,推导得到了四个噪声参数的解析闭合表达式。对于栅长 40 nm、尺寸为 4×5 μm(栅指数量×单位栅宽)的 MOSFET,仿真结果与实验数据表现出良好的一致性。

关 键 词:等效电路;MOSFET;参数提取;噪声模型;小信号模型

中图分类号:O43 **文献标识码**:A

Introduction

While MOSFET modeling is well-established for digital and low-frequency analog applications, extending these models to high-frequency domains introduces significant challenges. At RF (radio frequency) frequencies, understanding and modeling thermal noise become critical, as it emerges as the dominant noise source in MOSFETs [1-3]. Analytical expressions for noise parameters are essential for optimizing the noise performance of MOSFETs used in low-noise amplifiers. These expressions offer valuable insights into the underlying physical mechanisms and enable an assessment of how various parameters in the small-signal equivalent circuit impact performance [4-5].

However, modeling RF noise is complicated by its sensitivity to parasitic and coupling effects associated with the gate, transmission lines, pads, and lossy substrates [6-11, 14-17]. For GaAs FETs, Fukui [9] proposed an empirical relationship between the noise figure and circuit parameters using fitting coefficients. Similarly, A. Cappy developed simplified analytical formulas for the minimum noise figure, noise conductance, and optimal source impedance, based on a fundamental equivalent circuit that accounts for intrinsic gate-to-source capacitance and extrinsic gate and drain resistance [10].

This study introduces analytical formulas for the noise parameters of microwave MOSFETs, derived from a small-signal and noise-equivalent circuit model that incorporates the influence of extrinsic resistance. The paper is organized as follows: Section II details the noise-equivalent circuit model and the derivation of noise parameter expressions. Section III presents experimental findings, and Section IV concludes the study.

Received date: 2024-12-23, **revised date**: 2025-11-21 **收稿日期**:2024-12-23,**修回日期**:2025-11-21

Foundation items: Supported by the National Key R&D Program of China (2020YFB1807301), the National Natural ScienceFoundation of China (2024-MMT-07).

Biography: Gao Hanqi (2000-), male, Shanghai, PHD student. Research area involves mmW IC design. E-mail: gaohanqi@sjtu. edu. cn

* **Corresponding author**: E-mail: zhoujianjun@sjtu. edu. cn

1 Theory Analysis

1.1 Intrinsic equivalent circuit model

Figure 1 depicts the intrinsic small-signal and PRC (Pucel) noise-equivalent circuit model of the MOSFET. In this model, C_{gs} accounts for the combined gate-channel capacitance and gate-source overlap capacitance, while C_{gd} predominantly arises from the gate-drain overlap. The drain-to-source capacitance is represented by C_{ds}. Additionally, the transconductance is denoted by g_m, the drain conductance by g_{ds}, and τ represents the time delay associated with the transconductance.

The gate-induced noise current $\overline{i_{gs}^2}$ and the drain-channel noise current $\overline{i_{ds}^2}$ are represented by the following expressions [12]:

$$\overline{i_g^2} = 4kT\Delta f\omega^2 C_{gs}^2 R/g_m \quad , \quad (1)$$

$$\overline{i_d^2} = 4kT\Delta f g_m P \quad . \quad (2)$$

The cross correlation between $\overline{i_g^2}$ and $\overline{i_d^2}$ can be expressed as:

$$\overline{i_g i_d} = C\sqrt{\overline{i_g^2}\,\overline{i_d^2}} = 4kT\Delta f\omega C_{gs} C\sqrt{PR} \quad , \quad (3)$$

here, R and P represent the gate and drain noise model parameters, respectively, while C denotes the correlation coefficient.

Based on the noise correlation matrix method [13], the four noise parameters are derived as follows:

$$F_{min} = 1 + 2k_2 + \frac{\omega C_{gs}}{g_m k_1}\sqrt{PR(1-C^2)} \quad , \quad (4)$$

$$R_n = \frac{P}{g_m k_1} \quad , \quad (5)$$

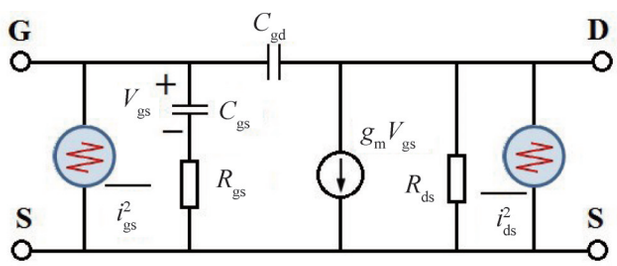

Fig. 1 Intrinsic noise model of MOSFET
图1 MOSFET本征噪声模型

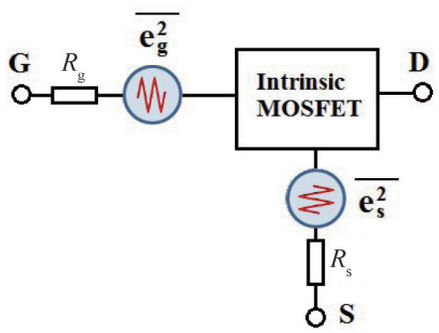

Fig. 2 Extrinsic resistance R_g and R_s noise model of MOSFET
图2 MOSFET的外延电阻 R_g 和 R_s 噪声模型

$$G_{opt} = \omega C_{gs}\sqrt{\frac{R}{P}(1-C^2)} \quad , \quad (6)$$

$$B_{opt} = -\omega[(C_{gs}+C_{gd}) - C\sqrt{\frac{R}{P}}C_{gs}] \quad , \quad (7)$$

where

$$k_1 = \frac{g_m + 2\omega^2 C_{gd}(\tau + C_{gs}R_{gs})}{g_m(1+\omega^2 C_{gs}^2 R_{gs}^2)} \quad , \quad (8)$$

$$k_2 = \frac{\omega^2 C_{gs}}{g_m k_1}\left[PC_{gs}R_{gs} - C\sqrt{PR}\left(\frac{C_{gd}}{g_m} + C_{gs}R_{gs} + \tau\right)\right] , \quad (9)$$

here, F_{min} represents the minimum noise factor, R_n is the noise resistance, Y_{opt} is the optimum source admittance, while G_{opt} and B_{opt} denote the optimum source conductance and susceptance, respectively.

1.2 Intrinsic equivalent circuit model of effect of R_g and R_s

The small-signal model incorporates three extrinsic resistances: R_g, which accounts for the distributed effects at the gate, and R_s and R_d, representing the source and drain resistances, respectively. These resistances are primarily influenced by the resistance of the lightly doped extensions of the source and drain diffusions. In the context of cascade noise figure calculations, R_g and R_s play crucial roles in determining the noise performance of the MOSFET, whereas the impact of R_d on noise performance is minimal and is typically negligible. Figure 2 illustrates the noise model of the MOSFET, emphasizing the extrinsic resistances R_g and R_s.

The two noise sources, $\overline{e_g^2}$ and $\overline{e_s^2}$ represent the noisy behavior of the access resistances R_g and R_s and are expressed as:

$$\overline{e_i^2} = 4kT_o qR_i\Delta f(i=g,s) \quad , \quad (10)$$

where q is the electronic charge, k is Boltzmann's constant, and T_o is the ambient temperature.

The corresponding chain noise correlation matrix can be expressed as follows:

$$C_A^{INT} = 4kT\begin{bmatrix} R_n + R_g + R_s & \frac{F_{min}-1}{2} - R_n(Y_{opt})^* \\ \frac{F_{min}-1}{2} - R_n Y_{opt} & R_n\left|Y_{opt}\right|^2 \end{bmatrix} \quad . \quad (11)$$

Therefore, the four noise parameters are given by:

$$R_n^{INT} = R_n + R_s + R_g \quad , \quad (12)$$

$$B_{opt}^{INT} = \frac{R_n B_{opt}}{R_n^{INT}} \quad , \quad (13)$$

$$G_{opt}^{INT} = \sqrt{\frac{R_n}{R_n^{INT}}(G_{opt})^2 + \frac{R_n R_g B_{opt}^2}{(R_n^{INT})^2}} \quad , \quad (14)$$

$$F_{min}^{INT} = F_{min} + 2(R_n^{INT}R_{opt}^{INT} - R_n G_{opt}) \quad , \quad (15)$$

When take no account of C_{gd} and g_{ds}, the above expressions are simplified as:

$$R_n = \frac{P}{g_m} + R_g + R_s \quad , \quad (16)$$

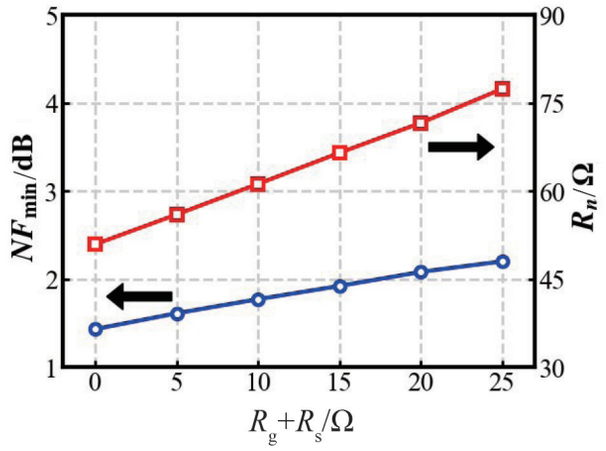

(a)

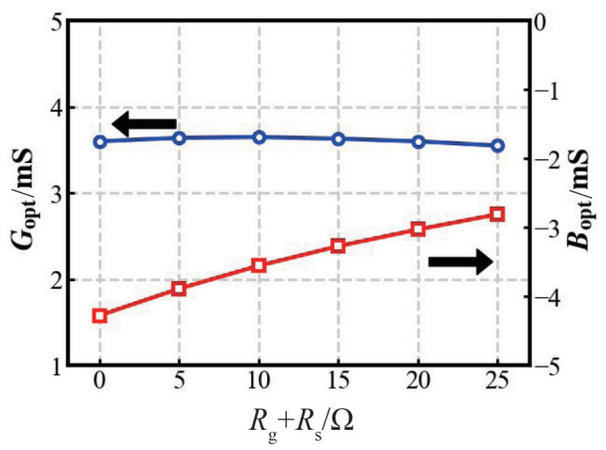

(b)

Fig.3　Noise parameters versus the sum of R_g and R_s (a) NF_{min} and R_n (b) G_{opt} and B_{opt}

图 3　噪声参数随 R_g 和 R_s 之和的变化关系(a) NF_{min} 和 R_n (b) Gopt 和 Bopt

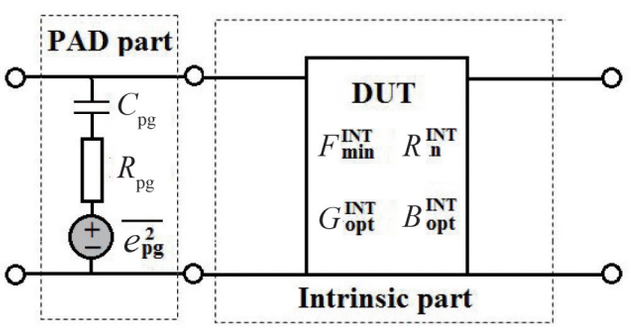

Fig. 4　Substrate resistance R_{pg} noise model of MOSFET

图 4　MOSFET 的衬底电阻 R_{pg} 噪声模型

$$B_{opt}=-\omega C_{gs}\frac{(P-C\sqrt{PR})}{P+(R_g+R_s)g_m}\quad,\quad(17)$$

$$C_A^t=4kT\begin{bmatrix}R_n^{INT} & \frac{F_{min}^{INT}-1}{2}-R_n^{INT}(Y_{opt}^{INT}-M)^*\\ \frac{F_{min}^{INT}-1}{2}-R_n^{INT}(Y_{opt}^{INT}-M) & R_n^{INT}(|Y_{opt}^{INT}|^2+|M|^2)\end{bmatrix}\quad,\quad(26)$$

$$G_{opt}=\omega C_{gs}\frac{\sqrt{(R_g+R_s)g_m(P+R-2C\sqrt{PR})+PR(1-C^2)}}{P+(R_g+R_s)g_m}\quad,\quad(18)$$

$$F_{min}=1+\frac{2\omega C_{gs}}{g_m}\sqrt{(R_g+R_s)g_m(P+R-2C\sqrt{PR})+PR(1-C^2)}\quad,\quad(19)$$

Figure 3 shows the noise parameters as a function of the sum (R_g+R_s). It can be observed that the minimum noise figure NF_{min} and the equivalent noise resistance R_n increase as (R_g+R_s) increases. The optimum source conductance G_{opt} remains roughly independent of (R_g+R_s), while the absolute value of the optimum source susceptance B_{opt} decreases with an increase in (R_g+R_s).

1.3　PAD parasitic

Figure 4 illustrates the substrate resistance R_{pg} noise model of the MOSFET. It can be seen that the pad parasitic consist of two elements: R_{pg} and C_{pg}. The parasitic associated with the pad due to substrate losses are represented by the capacitor C_{pg} in series with the resistor R_{pg}.

For shunt RC network (as shown in Fig. 4), the signal parameters can be expressed as follows:

$$A_{PAD}=\begin{bmatrix}1 & 0\\ M & 1\end{bmatrix}\quad,\quad(20)$$

with

$$M=\frac{j\omega C_{pg}}{1+j\omega R_{pg}C_{pg}}\quad,\quad(21)$$

It should be noted that the correlation noise matrices for series and shunt RC networks are non-zero because the two-port networks are passive and lossy.

$$C_Z^{PAD}=4kT\,\mathrm{Re}[Z_{PAD}]=4kTR_{pg}\begin{bmatrix}1 & 1\\ 1 & 1\end{bmatrix}\quad,\quad(22)$$

$$C_A^{PAD}=4kT\begin{bmatrix}0 & 0\\ 0 & N\end{bmatrix}\quad,\quad(23)$$

with

$$N=\frac{R_{pg}}{R_{pg}^2+1/(\omega C)^2}\quad,\quad(24)$$

In noise analysis applications involving the interconnection of two two-port networks, whether in cascade or otherwise, the resulting correlation matrix is related to the correlation matrices of the original two-port networks by [13]:

$$C_A^t=C_A^{PAD}+A_{PAD}C_A^{INT}A_{PAD}^+\quad,\quad(25)$$

It should be noted that a more complex relationship is obtained for the cascading connection of networks, which also includes the chain matrix A_{PAD} of the first two-port.

The corresponding correlation noise matrix in impedance representation can be expressed as follows:

$$R_n^{PAD} = R_n^{INT} \quad , \quad (27)$$

$$B_{opt}^{PAD} = B_{opt}^{INT} - \frac{\omega C_{pg}}{1 + (\omega R_{pg} C_{pg})^2} \quad , \quad (28)$$

$$G_{opt}^{PAD} = \sqrt{(G_{opt}^{INT})^2 + K\left(\frac{F_{min}^{INT}}{R_n^{INT}} - 2G_{opt}^{INT} + K\right)} \quad , \quad (29)$$

$$F_{min}^{PAD} = F_{min}^{INT} + 2R_n^{INT}(K + G_{opt}^{PAD} - G_{opt}^{INT}) \quad , \quad (30)$$

with

$$K = \frac{R_{pg}(\omega C_{pg})^2}{1 + (\omega R_{pg} C_{pg})^2} \quad , \quad (31)$$

From Eq. (27), it is evident that the equivalent noise resistance is independent of the pad parasitic. Figure 5 shows the three noise parameters as a function of R_{pg} and C_{pg}. It can be observed that the minimum noise figure NF_{min} increases with an increase in R_{pg} and C_{pg}, with a more significant effect observed for the pad capacitance C_{pg}. The optimum source conductance G_{opt} also increases with an increase in R_{pg} and C_{pg}. The optimum source susceptance B_{opt} remains independent of R_{pg} but increases with an increase in C_{pg}.

2 Experimental Verification

To validate the derived expressions for the extrinsic resistances, measurements were conducted on a 4 μm× 5 μm (number of gate fingers × unit gate width) NMOSFET with a 40 nm gate length, up to a frequency of 40 GHz for S-parameter characterization. High-frequency noise parameter measurements were performed on-wafer over the 8-26 GHz range using an ATN microwave noise measurement system.

2.1 PAD parasitic

Table 1 presents the MOSFET parasitic parameters, while Table 2 summarizes the extracted values of the small-signal elements at a constant drain-source voltage V_{DS} =1.2 V. Fig. 3 compares the measured and modeled S-parameters for the 4 μm×5 μm MOSFET across the fre-

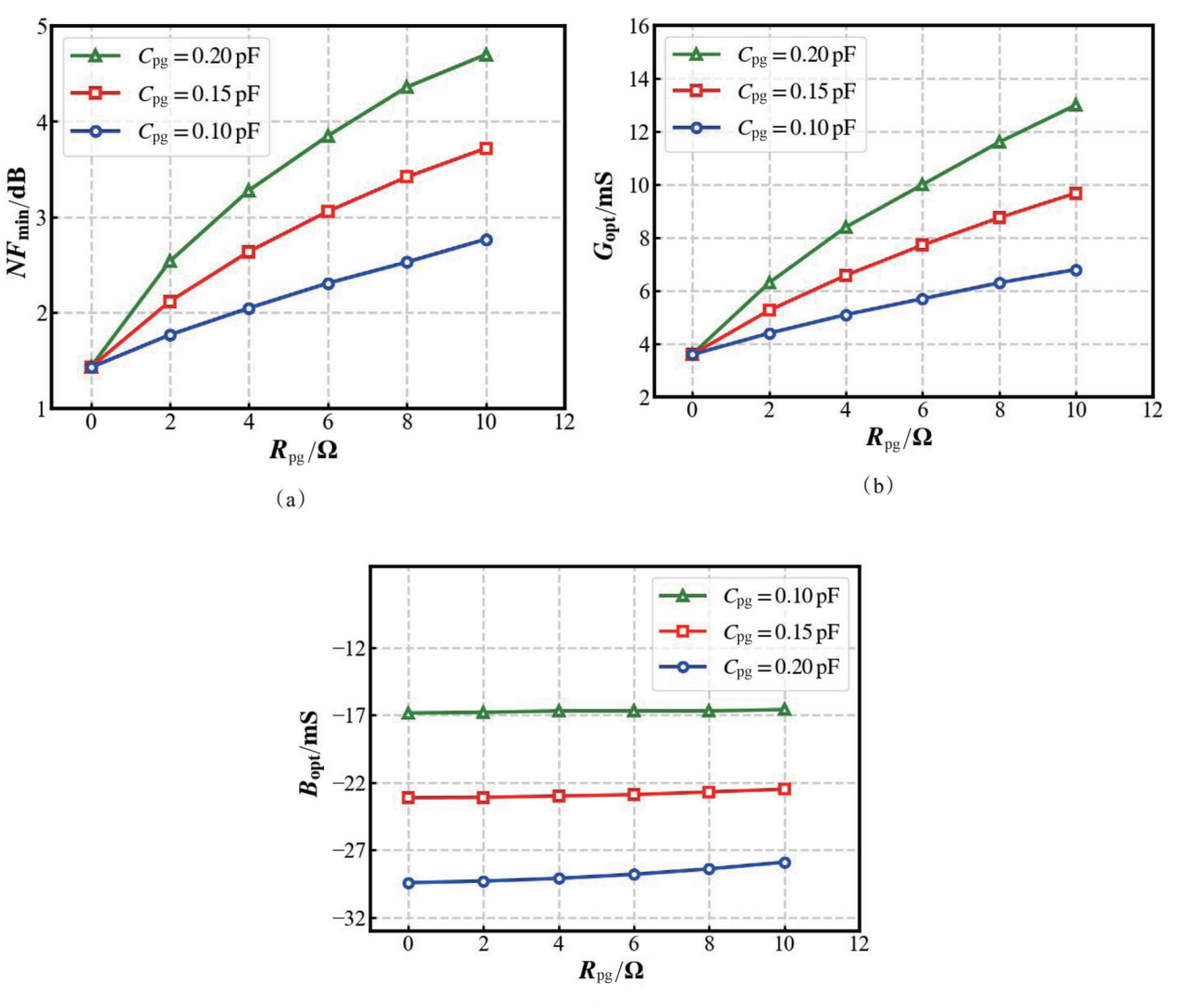

Fig.5 Noise parameters versus R_{pg} (a) NF_{min} (b) G_{opt} (c) B_{opt}
图5 噪声参数随 R_{pg} (a) NF_{min} (b) G_{opt} (c) B_{opt}变化图

Table 1　The MOSFET parasitic parameters
表 1　MOSFET 寄生参数

Parameters	Values	Units	Parameters	values	Units
C_{pg}	230	fF	R_g	30	Ω
C_{pd}	230	fF	R_d	5	Ω
C_{pgd}	2	fF	R_s	7	Ω
R_{pg}	4	Ω	R_{pd}	4	Ω

Table 2　Intrinsic parameters (V_{ds}=1.2 V)
表 2　本征参数(漏源电压 V_{ds} =1.2 V)

Parameters	Values	Parameters	Values
C_{gs} (fF)	55	C_{gd} (fF)	10
C_{ds} (fF)	25	R_{gs} (Ω)	15
g_m (mS)	54	g_{ds} (mS)	10

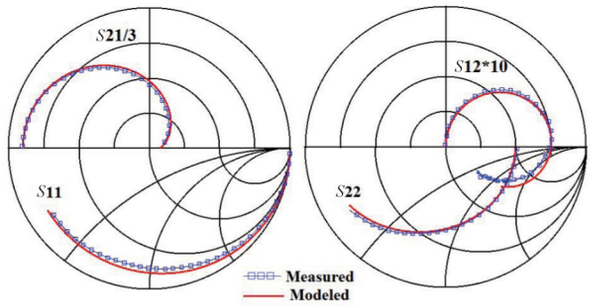

Fig. 6　Comparison of modeled and measured S parameters for the 4 μm×5 μm MOSFET. Bias: V_{gs}=1.2 V, V_{ds}=1.2 V
图 6　4×5 μm MOSFET 建模 S 参数和测试 S 参数对比. 偏置条件: V_{gs}=1.2 V, V_{ds}=1.2 V

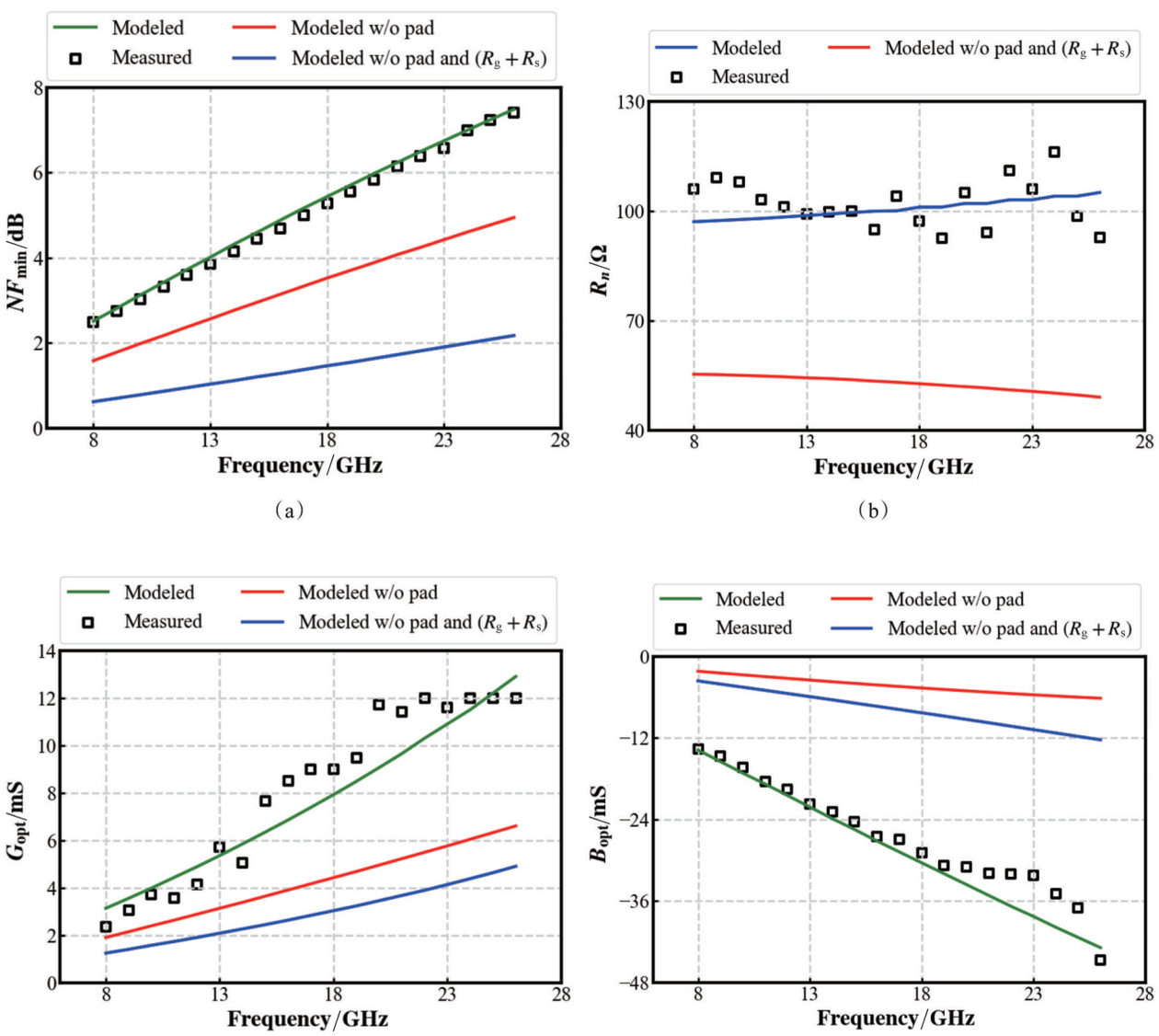

Fig. 7　Comparison of measured and modeled noise parameters for the 4 μm×5 μm MOSFET. Bias: V_{gs}=1.2 V, V_{ds}=1.2V (a) NF_{min} (b) R_n (c) G_{opt} (d) B_{opt}
图 7　4 μm×5 μm MOSFET 建模 *S* 参数和测试 *S* 参数对比. 偏置条件: V_{gs}=1.2 V, V_{ds}=1.2V (a) NF_{min} (b) R_n (c) G_{opt} (d) B_{opt}

quency range of 1 GHz to 40 GHz. The modeled S-parameters show excellent agreement with the measured data, validating the accuracy of the model.

2.2 Noise model verification

Figure 6 shows the comparison between the measured and modeled noise parameters for the 4 μm×5 μm MOSFET under the bias conditions V_{GS} =1.2 V and V_{DS} = 1.2 V, demonstrating excellent agreement across the entire frequency range.

Figure 7 presents a comparison of measured and simulated noise parameters, confirming the validity of the proposed method through strong agreement. As shown in Fig. 7(a), the influence of the pad and the combined resistances R_g and R_s on the minimum noise figure NF_{min} is evident. To minimize NF min , it is crucial to keep R_g and R_s as low as possible. In Fig. 7(b), it can be seen that the equivalent noise resistance R_n is affected by R_g and R_s. Fig. 7(c) shows that the impact of R_g and R_s on the optimum source conductance G_{opt} is minimal. Lastly, due to the large pad capacitance C_{pg} (exceeding 200 fF), the effect of C_{pg} on the optimum source susceptance B_{opt} is significant, as illustrated in Fig. 7(d).

3 Conclusions

This paper introduces an approach for analyzing the impact of extrinsic resistances on the noise performance of deep submicron MOSFETs. Analytical expressions for the noise parameters of microwave MOSFETs are derived using a small-signal and noise equivalent circuit model that incorporates the effects of extrinsic resistances. Excellent agreement is achieved between simulated and measured results up to 26 GHz for 4 μm×5 μm (number of gate fingers × unit gate width) MOSFETs with a 40 nm gate length.

References

[1] POSPIESZALSKI M W. Interpreting transistor noise[J]. IEEE Microwave Magazine, 2010, 11(6): 61-69.

[2] CHENG Y, DEEN M J, CHEN C H. MOSFET modeling for RF IC design[J]. IEEE Transactions on Electron Devices, 2005, 52(7): 1286-1303.

[3] GAO J. Direct parameter-extraction method for MOSFET noise model from microwave noise figure measurement[J]. Solid-State Electronics, 2011, 63(1): 42-48.

[4] GAO H, JIN J, ZHOU J. An approach to determine noise model parameter for submicron MOSFET from RF noise figure measurement [J]. IEEE Journal of the Electron Devices Society, 2024, 12: 692-697.

[5] WANG S C, CHEN K M, LIAO K H, et al. Comprehensive noise characterization and modeling for 65-nm MOSFETs for millimeter-wave applications[J]. IEEE Transactions on Microwave Theory and Techniques, 2010, 58(4): 740-746.

[6] GAO J, WERTHOF A. Scalable small signal and noise modeling for deep submicron MOSFETs[J]. IEEE Transactions on Microwave Theory and Techniques, 2009, 57(4): 737-744.

[7] GUO J C, LIN Y M. A new lossy substrate de-embedding method for sub-100 nm RF CMOS noise extraction and modeling[J]. IEEE Transactions on Electron Devices, 2006, 53(2): 339-347.

[8] ZHANG H, NIU G, LIANG Q, et al. Extraction of drain current thermal noise in a 28 nm high-k/metal gate RF CMOS technology[J]. IEEE Transactions on Electron Devices, 2018, 65(6): 2393-2399.

[9] FUKUI H. Design of microwave GaAs MESFET's for broadband low-noise amplifier[J]. IEEE Transactions on Microwave Theory and Techniques, 1979, 27(7): 643-650.

[10] CAPPY A. Noise modeling and measurements techniques[J]. IEEE Transactions on Microwave Theory and Techniques, 1988, 36(1): 1-10.

[11] ASGARAN S, DEEN M J, CHEN C H, et al. Analytical determination of MOSFET's high-frequency noise parameters from NF50 measurements and its application in RFIC design[J]. IEEE Journal of Solid-State Circuits, 2007, 42(5): 1034-1043.

[12] PUCEL R A, HAUS H A, STATZ H. Signal and noise properties of GaAs microwave FET[M]//MORTON L. Advances in Electronics and Electron Physics. New York: Academic Press, 1975: 35-98.

[13] HILLBRAND H, RUSSER P H. An efficient method for computer-aided noise analysis of linear amplifier networks[J]. IEEE Transactions on Circuits and Systems, 1976, 23(4): 235-238.

[14] PANDA D K, LENKA T R. Investigation of gate induced noise in E-mode GaN MOS-HEMT and its effect on noise parameters[J]. International Journal of Numerical Modelling: Electronic Networks, Devices and Fields, 2018, 31(5): e2318.

[15] JENA B, DASH S, MISHRA G P. Effect of underlap length variation on DC/RF performance of dual material cylindrical MOS[J]. International Journal of Numerical Modelling: Electronic Networks, Devices and Fields, 2017, 30(5): e2175.

[16] BANERJEE S, GHOSH M, MONDAL P, et al. Third order inverse multifunction filter employing MOS resistors and capacitors[J]. International Journal of Numerical Modelling: Electronic Networks, Devices and Fields, 2022, 35(5): e3002.

[17] VISWANATHAN S, PRAVIN C, ARASAMUDI R B, et al. Influence of interface trap distributions over the device characteristics of AlGaN/GaN/AlInN MOS-HEMT using Cubic Spline Interpolation technique[J]. International Journal of Numerical Modelling: Electronic Networks, Devices and Fields, 2022, 35(1): e2936.